Robotica (2026), **44**, pp. 195–209
doi:10.1017/S0263574725103044

CAMBRIDGE UNIVERSITY PRESS

RESEARCH ARTICLE

Load-adaptive control for quadruped mobile manipulation platforms

Zeyu Cai, Ruipeng Cai, Zhentao Xie, Ning Huang and Qinchuan Li

School of Mechanical Engineering, Zhejiang Sci-Tech University, Hangzhou, 310018, China
Corresponding Author: Qinchuan Li; Email: lqchuan@zstu.edu.cn

Received: 26 September 2025; **Revised:** 18 November 2025; **Accepted:** 27 November 2025;
First published online: 2 February 2026

Keywords: adaptive control; model predictive control; whole-body control; quadruped robots; unknown impact model

Abstract

Currently, quadruped robots are widely used in diverse scenarios due to their high mobility, creating a demand for more advanced interaction capabilities. This study proposes a whole-body planning and control framework that integrates adaptive control into a hierarchical model predictive control (MPC) and whole-body control (WBC) structure, enhancing the environmental adaptability and interaction performance of quadruped mobile manipulators. Key innovations include: a recursive least squares and feedforward compensation strategy for accurate end-effector force estimation; relaxed barrier functions embedded in the MPC to combine dynamic obstacle avoidance with adaptive control; and a WBC-based priority hierarchy to enforce critical constraints. Validated in Gazebo simulation and on the B1-Z1 platform, the method allows the robot to handle unknown loads up to 3 kg and maintain tracking errors under 2 cm despite 35 N external disturbances. It also demonstrates strong adaptability in non-uniform object transportation, providing a reliable solution for unstructured environments.

1. Introduction

The quadrupedal mobile manipulation platform [1] comprises a quadruped robotic base and an onboard manipulator. This integrated system leverages the complex terrain adaptability of legged robots and the interactive manipulation capabilities of robotic arms [2], demonstrating considerable potential for high-value applications such as industrial inspection [3, 4] and disaster rescue [5, 6]. From a mechanistic perspective, the quadrupedal robot itself can be considered a mobile platform with six degrees of freedom; when combined with a manipulator, it constitutes a resilient machine [7] with kinematic redundancy. However, in existing control methodologies, the mobile platform and the manipulator are often treated as independent subsystems, relying on complex high-level monitoring systems to adjust their motions separately. Although this approach achieves a degree of functional redundancy, it neglects the kinematic and dynamic coupling effects between the two components, resulting in a control architecture that is rigid, complex, and ultimately limits global coordination and operational flexibility. Some approaches attempt to adapt task-space control strategies originally designed for wheeled platforms [8], simplifying the quadruped robot into a virtual six-degree-of-freedom platform. However, such simplification neglects leg–ground contact dynamics, particularly in high-payload configurations or cases where leg inertia contributes significantly to system dynamics, thereby undermining overall robustness and terrain adaptation. Therefore, it is essential to treat the mobile platform and the manipulator as a unified system and achieve coordinated operation between them.

To address the aforementioned challenges, a control algorithm capable of achieving coordinated operation is required. Convex model predictive control (MPC) based on the single rigid body (SRB) model has been demonstrated to be effective for real-time multi-gait generation in legged robots [9].

© The Author(s), 2026. Published by Cambridge University Press.

https://doi.org/10.1017/S0263574725103044 Published online by Cambridge University Press

In contrast to traditional quadratic programming (QP)-based balance controllers [10], this MPC framework can support highly dynamic behaviors such as jumping [9, 11] and high-speed bounding [12]. In recent years, integration of MPC with other methods has advanced motion trajectory tracking, such as LPV-MPC [13], achieving global linearization through scheduling variables for efficient wheeled robot control. However, quadruped mobile manipulation platforms face more complex dynamics due to inertial coupling and mass effects, where simplified SRB models lead to mismatch in dynamic gaits or load changes.

To address this, our study employs a whole-body dynamics-based nonlinear MPC that incorporates full limb-manipulator coupling for coordinated optimization, ensuring precise tracking and stability in complex scenarios. In recent years, MPC schemes utilizing full rigid-body dynamics models have achieved progress in hardware implementation. For example, Katayama et al. [14] and Mastalli et al. [15] accelerated the solution of differential dynamic programming through inverse dynamics modeling. A representative case is the MPC strategy adopted in ref. [16], which employs a 100-step prediction horizon (with a 10-ms time resolution) and runs at 50 Hz. However, the computational burden of full-body dynamics MPC typically limits its update frequency to 50–100 Hz (for 12-degree-of-freedom quadrupedal systems), making it challenging to meet the demands of highly dynamic tasks. To overcome this limitation, a hierarchical control architecture has been widely adopted. In this architecture, the planning layer utilizes full-body dynamics-based MPC to generate reference trajectories (updated at 50–100 Hz), while the tracking layer employs an operational-space inverse dynamics-based whole-body control (WBC) method. This WBC scheme solves a constrained QP problem to compute joint torques, thereby achieving compliant trajectory tracking at an update rate of 1 kHz [17–20].

Building upon the aforementioned motion control algorithms, Jean-Pierre Sleiman et al. [21] proposed a unified multi-contact optimal control framework. This framework models both arms and legs as generalized contact limbs, constructing an augmented model that incorporates the dynamics of the manipulated object, the centroidal dynamics of the robot, and its full kinematics. This design enables the unified encoding of both robot-centric and object-centric tasks. This approach treats the quadrupedal robot and the manipulator as a unified system. This integrated framework enables task-adaptive coordination, allowing for dynamic motion redistribution between the mobile base and the arm to fully exploit the functional redundancy of the resilient machine [7]. A key limitation of this method, however, is its dependence on predefined physical parameters (mass, inertia) of the object. This requirement prevents it from adapting to scenarios with unknown payloads. When grasping objects with unknown properties, the trajectory tracking accuracy at the end-effector degrades significantly, which can even lead to systemic instability.

To enable the mobile manipulation platform to fully utilize its payload manipulation capabilities and effectively operate in complex, dynamic, and unstructured environments, this paper proposes a novel control algorithm. The main contributions of this study are summarized as follows:

- A sensorless disturbance observer design that constructs an external force disturbance solver based on deviations between the robot's actual and reference states, combining the update frequency differences between MPC (low-frequency) and WBC (high-frequency) to propose a fast adaptive control algorithm that demonstrates strong robustness against heterogeneous loads (e.g., partially-filled liquid containers or suspended weights) while enabling real-time external disturbance estimation without requiring additional force sensors.
- An unknown payload adaptive control framework that integrates whole-body dynamics, kinematic constraints, and disturbance observation to ensure end-effector trajectory tracking stability when grasping objects with completely unknown physical properties.
- The payload-adaptive control system was implemented on a Unitree B1 quadruped robot with a Z1 7-DoF arm. Experiments show that: (i) the adaptive system demonstrates stability when subjected to unknown payloads of up to 35 N. This capability allows the system to fully utilize the manipulator's performance, which is rated for a maximum payload of 3 kg [22]; (ii) in simulation,

https://doi.org/10.1017/S0263574725103044 Published online by Cambridge University Press

the non-adaptive system lost stability at 25N, while the adaptive system withstood 35N; (iii) the adaptive platform successfully achieved precise grasping and transportation of 2.5 kg objects.

The structure of this paper is as follows. Section 2 introduces the basic MPC-WBC algorithm framework. Section 3 investigates the estimation of external forces from robot state deviations. Section 4 describes the integration of the force estimation algorithm into the MPC-WBC framework for stable robot control. Section 5 validates the proposed method with five groups of simulations and physical experiments. Conclusions are provided in Section 6.

2. Preliminaries

The quadrupedal mobile manipulation platform employs a hierarchical control framework as shown in Figure 1, consisting of five core modules [14]: the whole-body planner (based on MPC), whole-body controller (based on WBC), low-level joint controller, state estimator, and gait scheduler. Based on user commands and state estimation, the gait scheduler generates contact sequences; the MPC-based whole-body planner solves for reference trajectories; the whole-body controller computes desired joint torques; and the low-level controller executes torque-current conversion. The whole-body planner and whole-body controller together form the high-level control core, upon which the adaptive controller proposed in this work is constructed (see Section 4 for details).

2.1. Whole-body planner (based on MPC)

We formulate the optimal control problem as follows:

$$\begin{cases} \min\limits_{u} & \Phi(x(T)) + \int_0^T L(x(t), u(t), t)dt \\ s.t. & \dot{x}(t) = f(x(t), u(t), t) \\ & g(x(t), u(t), t) = 0 \\ & h(x(t), u(t), t) \geq 0 \\ & x(0) = x_0, \end{cases} \tag{1}$$

where $x(t)$ and $u(t)$ represent the state vector and input vector at time step t, while $L(x(t), u(t), t)$ and $\Phi(x(T))$ denote the stage cost and terminal cost functions. Our objective is to find a control sequence that minimizes the total cost under the constraints of initial state x_0, system dynamics $\dot{x}(t) = f(x(t), u(t), t)$, equality constraints $g(\cdot)$, and inequality constraints $h(\cdot)$.

2.1.1. System dynamics

This research addresses the dynamic control problem of quadrupedal mobile manipulation platforms using a whole-body centroidal dynamics modeling approach. Following the conclusions in ref. [8], we emphasize that for quadrupedal systems equipped with multi-degree-of-freedom manipulators, the influence of leg mass distribution on system dynamics must be properly accounted for, rather than adopting the simplified massless limb assumption. The derived centroidal dynamics equation is expressed as:

$$\dot{p}_G = \sum_{i=1}^{n_c} \lambda_i + mg \tag{2a}$$

$$\dot{l}_G = \sum_{i=1}^{n_c} r_{Gi} \times \lambda_i \tag{2b}$$

The robot state $x = (h_G, q_b, q_j) \in \mathbb{R}^{12+n_a}$ comprises the centroidal momentum h_G, base pose q_b, and joint positions q_j. The centroidal momentum $h_G = (p_G, l_G) \in \mathbb{R}^6$ consists of linear momentum p_G and

https://doi.org/10.1017/S0263574725103044 Published online by Cambridge University Press

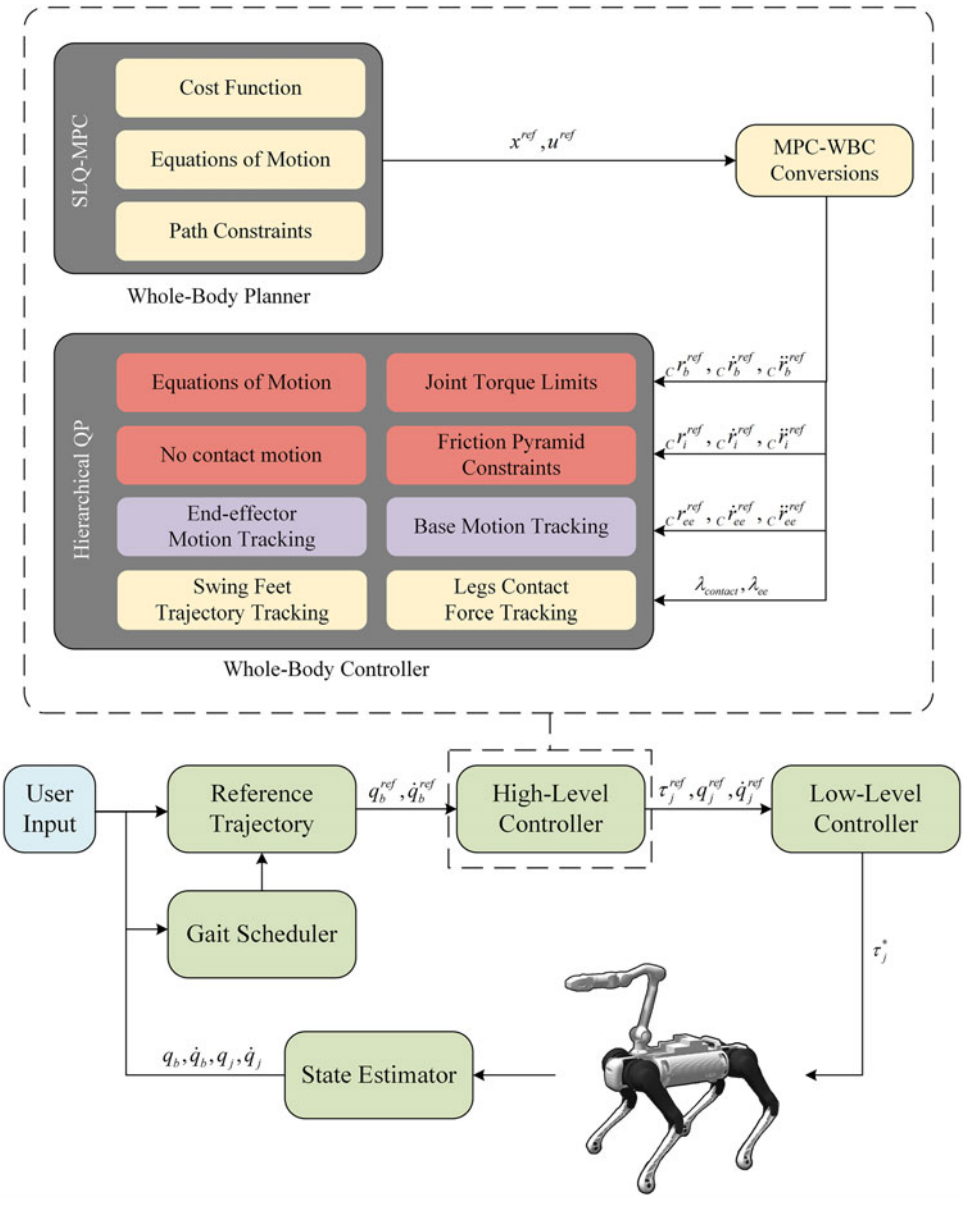


Figure 1. *The diagram outlines the key elements of the fully actuated control architecture.*

angular momentum l_G. The input vector $u = (\lambda_i, \cdots, \lambda_{n_c}, v_j) \in \mathbb{R}^{3n_c+n_a}$ includes contact forces λ_i at n_c contact points and joint velocities v_j, where r_{Gi} denotes the position vector from the i-th contact point to the centroid.

2.1.2. Cost function

We encode all robot-centric and end-effector-centric tasks into a unified cost function formulated as:

$$L(x(t), u(t), t) = \left\| x_r - x_r^{ref} \right\|_{Q_r}^2 + \left\| u - u^{ref} \right\|_R^2 + \left\| r_{IE} - r_{IE}^{ref} \right\|_{Q_{eep}}^2 + \left\| \xi_{IE} \right\|_{Q_{eeo}}^2 \tag{3}$$

where R are positive definite matrices; $Q_r, Q_{eep}, Q_{eeo}$are positive semi-definite weighting matrices; $r_{IE}, \xi_{IE} \in \mathbb{R}^3$ represent the end-effector's position and orientation errors respectively.

https://doi.org/10.1017/S0263574725103044 Published online by Cambridge University Press

2.1.3. Constraint functions

These constraints capture the distinct modes of each leg at any given time. Assuming the mode sequence is a predefined temporal function, we denote by $N_{contact}$ the set of all closed contacts during time period. The resulting constraints are expressed as:

$$\begin{cases} v_i\,(x,u) = 0, f_c(\mu_c)\cdot\lambda_i \geq 0, & if\ i \in N_{contact}, \\ v_i(x,u)\cdot\hat{n} = s(t), \lambda_i = 0, & if\ i \notin N_{contact}, \end{cases} \tag{4}$$

where v_i denotes the foot-end velocity in the world coordinate frame, enforcing that: (1) stance legs maintain ground contact through $v_i = 0$; (2) swing legs follow the predefined trajectory $s(t)$ along the local surface normal direction $\hat{n} \in \mathbb{R}^3$. Additionally, zero contact force is enforced for swing legs, while stance legs are subject to friction cone constraints $f_c(\mu_c)$ defined by the surface normal $\hat{n}$ and friction coefficient $\mu_c = 0.7$.

2.2. Whole-body controller (based on WBC)

The whole-body controller employs a hierarchical optimization architecture to track reference trajectories for both the base and limbs. This controller solves for optimal generalized accelerations and contact forces through QP formulation with prioritized tasks [23, 24], subsequently computing joint torques via inverse dynamics. The specific task prioritization scheme is illustrated in Figure 1.

2.2.1. Equations of motion

The mechanical system's equations of motion establish the relationship between generalized acceleration $\dot{u}_{WBC}$, contact forces λ_c, and joint torques τ. By defining $x_{WBC} = [\,\dot{u}_{WBC}\ \lambda_c\,]^T$, the robot's centroidal dynamics model takes the following form:

$$\left[M_b(q)\ -J_b^T\right]\cdot x_{WBC} = -h_b(q,\dot{q}) \tag{5}$$

where $(\cdot)_b$ denotes base-related components in parameter matrices.

2.2.2. No contact motion

To ensure contact consistency for stance legs (which are constrained from moving), the following tasks must be enforced:

$$\left[J_i\ 0_{3\times n_a}\right]\cdot x_{WBC} = -\dot{J}_i\cdot u_{WBC}, \sim i \in N_{contact} \tag{6}$$

2.2.3. Torque limits

To enforce joint torque limitations within hardware-specified bounds, we formulate the following joint torque constraint task:

$$\begin{bmatrix} M_j(q) & -J_j^T \\ -M_j(q) & J_j^T \end{bmatrix}\cdot x_{WBC} \leq \begin{pmatrix} \tau_{\max}\cdot 1_{n_a\times 1} - h_j(q,\dot{q}) \\ -\tau_{\min}\cdot 1_{n_a\times 1} + h_j(q,\dot{q}) \end{pmatrix} \tag{7}$$

where $1_{n_a\times 1} = [\,1\ \cdots\ 1\,]^T \in \mathbb{R}^{n_a}$, $(\cdot)_j$ denotes joint-related components in parameter matrices.

2.2.4. Friction pyramid constraint

To prevent slippage, the contact force $\lambda_c \in \mathbb{R}^{3\times n_c}$ generated by the i-th foot must be constrained within the friction cone. To obtain a linear formulation, we approximate the friction cone using a pyramid. Thus, given the friction coefficient μ_c, the friction constraint for the i-th leg's contact force can be expressed as:

$$f_c(\mu_c)\cdot\lambda_i = \begin{bmatrix} 1 & 0 & \mu_c \\ 1 & 0 & -\mu_c \\ 0 & 1 & \mu_c \\ 0 & 1 & -\mu_c \\ 0 & 0 & 1 \end{bmatrix}\cdot\lambda_i \geq 0,\quad i \in N_{contact} \tag{8}$$

https://doi.org/10.1017/S0263574725103044 Published online by Cambridge University Press

2.2.5. Trajectory tracking

After ensuring dynamic feasibility, hardware torque limits, and non-slipping contact constraints, we perform trajectory tracking for the center of mass (CoM), swing legs, and end-effector [25, 26]. Given reference CoM trajectories ${}_C r_b^{ref}$,${}_C \dot{r}_b^{ref}$ and ${}_C \ddot{r}_b^{ref}$ in the operational space, the tracking is implemented as follows [8]:

$$\left[{}_C J_b \; 0_{6\times n_a} \right] \cdot x_{WBC} = {}_C \ddot{r}_b^{ref} + K_{p,b} \cdot {}_C \tilde{r}_b + K_{d,b} \cdot {}_C \dot{\tilde{r}}_b - {}_C \dot{J}_b \cdot u_{WBC} \tag{9a}$$

Similarly, trajectory tracking for both the swing legs and the robotic arm's end-effector can also be achieved using the above formulation; therefore, we define:

$$\left[{}_C J_i \; 0_{3\times n_a} \right] \cdot x_{WBC} = {}_C \ddot{r}_i^{ref} + K_{p,i} \cdot {}_C \tilde{r}_i + K_{d,i} \cdot {}_C \dot{\tilde{r}}_i - {}_C \dot{J}_i \cdot u_{WBC}, \quad i \notin N_{contact} \tag{9b}$$

$$\left[{}_C J_{ee} \; 0_{6\times n_a} \right] \cdot x_{WBC} = {}_C \ddot{r}_{ee}^{ref} + K_{p,ee} \cdot {}_C \tilde{r}_{ee} + K_{d,ee} \cdot {}_C \dot{\tilde{r}}_{ee} - {}_C \dot{J}_{ee} \cdot u_{WBC} \tag{9c}$$

2.2.6. Contact force tracking

We execute contact force tracking with the lowest priority, which guides the contact force solution while ensuring the primary task objectives proceed unimpeded, thereby accelerating the overall solver convergence.

$$\left[0_{n_a\times(12+n_a)} \; \mathrm{I}_{n_a\times n_a} \right] \cdot x_{WBC} = \lambda^{ref} \tag{10}$$

where λ^{ref} represents the ideal contact force computed by the MPC solver.

3. External force estimation algorithm

This section presents a novel robotic external force estimation method based on recursive least squares with forgetting factor (RLS-FF), which achieves real-time interaction force estimation through fusion of dynamic models and joint sensor data. The proposed approach incorporates an enhanced forgetting factor mechanism that significantly improves estimation accuracy and response speed in dynamic environments.

3.1. External force estimation model

For floating-base robotic systems, we first establish the standard dynamic equation:

$$M(q)\ddot{q} + h(q, \dot{q}) = \tau + J^T(q)\lambda \tag{11}$$

By defining the nominal state dynamics (external-force-independent terms) on the left-hand side as: $\tau_d = M(q)\ddot{q} + h(q, \dot{q})$, the dynamic equation simplifies to an external-force-explicit form:

$$\lambda = J^{-T}(q)(\tau_d - \tau) \tag{12}$$

In practical systems, accounting for noise interference in joint torque measurements and state estimations, we introduce joint torque residual $\delta\tau = \tau - \hat{\tau}$ and state residual $\delta\tau_d = \tau_d - \hat{\tau}_d$, where $\hat{\tau}$ and $\hat{\tau}_d$represent the measured values of joint torques and dynamic terms, respectively, yielding the disturbance equation:

$$\hat{\tau}_d + \delta\tau_d = \hat{\tau} + \delta\tau + J^T(q)\lambda \tag{13}$$

Assuming the system noise follows Gaussian distributions: $\delta\tau_d \sim \mathrm{N}(0, R_d), \delta\tau \sim \mathrm{N}(0, R)$, where $\{R_d, R\}$ are their respective covariance matrices. By merging the measurement noise terms, we ultimately construct an observation model incorporating noise characteristics:

$$e = J^T(q)\,\lambda - \tau^\circ \tag{14}$$

where $\tau^\circ = \hat{\tau}_d - \hat{\tau}$ represents the observed value of the nominal state, and $e = \delta\tau_d \oplus \delta\tau$ denotes the system noise. The "$\oplus$" symbol indicates probabilistic superposition between $\delta\tau_d$ and $\delta\tau$. This model

https://doi.org/10.1017/S0263574725103044 Published online by Cambridge University Press

probabilistically combines the nominal state observation with system noise, establishing a theoretical foundation for subsequent parameter estimation.

3.2. External force estimation model

The external force estimation problem is transformed into a noise energy minimization process for dynamic systems. Based on the weighted least squares criterion, an optimization objective function incorporating a forgetting factor is constructed:

$$\lambda(t_N) = \arg\min_{\lambda} \left(\sum_{k=1}^{N} \alpha^{N-k} \left\| e(t_k) \right\|_W^2 \right) \tag{15}$$

where $\alpha \in (0, 1]$ is the forgetting factor, which exponentially weights and decays the influence of historical data; N represents the observation window length, reflecting the time constant of the system's dynamic characteristics. This weighted least squares problem is solved in real-time using the RLS method, with its iterative form given by:

$$\begin{cases} K_{ef}\left(t_k\right) = \dfrac{P_{ef}\left(t_{k-1}\right) \cdot \left(J^T\left(t_k\right)\right)^T}{\alpha \cdot E_{(6+n_a)\cdot(6+n_a)} + J^T\left(t_k\right) \cdot P_{ef}\left(t_{k-1}\right) \cdot \left(J^T\left(t_k\right)\right)^T} \\ \lambda(t_k) = \lambda(t_{k-1}) + K_{ef}\left(t_k\right) \cdot \left(\tau^{\circ}\left(t_k\right) - J^T\left(t_k\right) \cdot \lambda\left(t_{k-1}\right)\right) \\ P_{ef}(t_k) = \dfrac{P_{ef}(t_{k-1}) - K_{ef}\left(t_k\right) \cdot J^T(t_k) \cdot P_{ef}\left(t_{k-1}\right)}{\alpha} \end{cases} \tag{16}$$

Here, $P_{ef}(t_k)$ is the error covariance matrix, $K_{ef}(t_k)$ is the Kalman gain matrix, and $E_{(6+n_a)\cdot(6+n_a)}$ is the identity matrix. Finally, the estimated generalized interaction force $\tilde{\lambda}_{ee} = [\tilde{f}_{ee}\ \tilde{\tau}_{ee}]^T \in \mathbb{R}^6$ at the robot's end-effector can be directly extracted from the last six elements of $\lambda(t_k)$, corresponding to the contact force and torque components.

3.3. The α-adaptive method based on control architecture

The RLS-FF algorithm serves as an efficient online parameter estimation method, particularly suitable for time-varying robotic dynamic parameters. By recursively updating parameters, this method introduces a forgetting factor α to exponentially decay the weight of historical data, thereby assigning higher confidence to new data and enabling effective tracking of time-varying parameters. The value of α critically impacts estimation performance: as α approaches 0, the algorithm exhibits strong tracking capability but increased noise sensitivity, leading to amplified estimation variance and parameter oscillation; as α approaches 1, it demonstrates excellent noise resistance but noticeable parameter update lag.

Conventional force estimation methods typically employ a fixed forgetting factor, which suffers from two major limitations: (1) difficulty in adapting to rapid parameter variations in dynamic interaction scenarios, and (2) failure to fully leverage the hierarchical nature of the control architecture. In contrast, the deep coupling framework proposed in this study adopts a dual-time-scale estimation strategy, enabling high-frequency parameter fine-tuning at the WBC layer (1 kHz) and low-frequency parameter reconstruction at the MPC layer (50–100 Hz), thereby significantly improving system adaptability. Within the MPC-WBC hierarchical control architecture, the MPC module optimizes and generates reference joint trajectories over a finite time horizon, while the WBC module performs local optimization at a higher frequency to achieve accurate trajectory tracking based on the commands from MPC. This division of labor implies that each time MPC updates its planned trajectory, the reference for the WBC module changes, thereby reducing the relevance of previously accumulated historical data for force estimation at the current moment. Accordingly, our method proactively reduces the forgetting factor in the RLS algorithm after each MPC update. This deliberate reduction diminishes the weight of older data,

https://doi.org/10.1017/S0263574725103044 Published online by Cambridge University Press

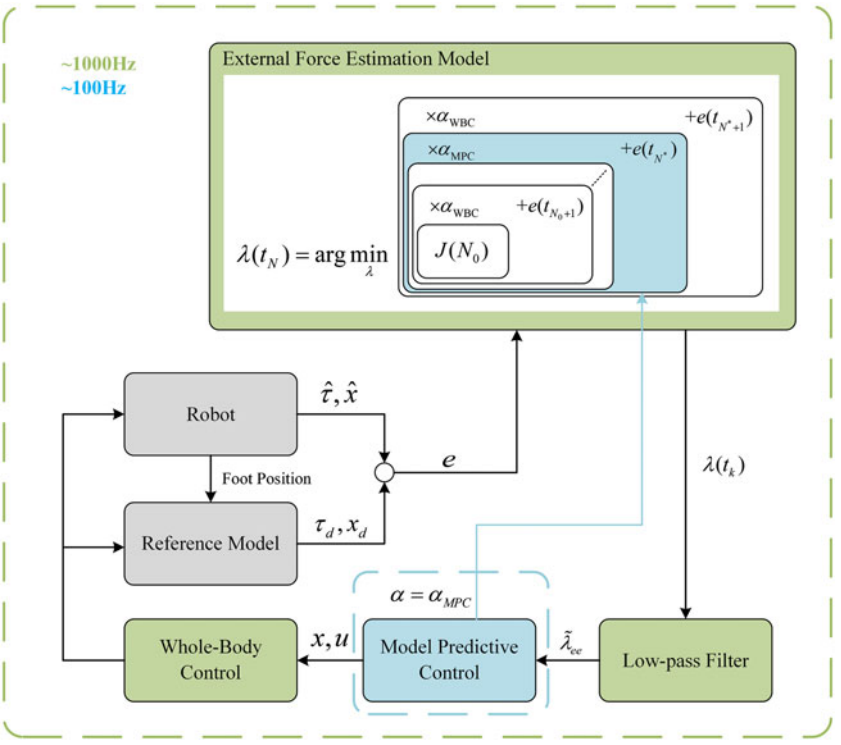


Figure 2. *Block diagram of the proposed adaptive force-based controller.*

allowing the estimator to adapt more rapidly to dynamic variations introduced by the new trajectory commands. Compared to strategies with a fixed forgetting factor, this approach aligns more naturally with the decision-making cycle of the controller, enhancing the response speed to load variations while maintaining estimation stability.

As shown in the control framework (Figure 2), within each control cycle (1 kHz): (1) the WBC first solves for joint torque commands and sends them to the low-level controller; (2) the force estimator then updates dynamic parameters using the RLS-FF algorithm (computational complexity $O(n^2)$) based on discrepancies between actual states and the reference model; (3) the refined parameters are applied to the next cycle's WBC computation.

Under the synchronous framework, the forgetting factor is set as $\alpha = \alpha_{WBC}$. Furthermore, since the WBC algorithm operates at a fixed control cycle, Equation (15) is reformulated as $\lambda(N) = \arg\min_{\lambda}\left(\sum_{k=1}^{N} \alpha_{WBC}^{N-k}\|e(k)\|_W^2\right)$, where N denotes the number of cycles. Assuming $J(N) = \sum_{k=1}^{N} \alpha_{WBC}^{N-k}\|e(k)\|_W^2$, we derive:

$$J(N) = \left[\alpha_{WBC}^{N-1}\cdot e^2(1) \cdots \alpha_{WBC}^{1}\cdot e^2(N-1)\ e^2(N)\right]\cdot 1_{N\times 1} \tag{17}$$

To address the lower update frequency of MPC (100 Hz), a dynamic forgetting factor adjustment strategy is designed: During each MPC policy update, the forgetting factor is automatically reduced to diminish historical data weighting, thereby enhancing the algorithm's rapid response capability to new policies. This design ensures stable estimation within MPC cycles while maintaining adaptability to parameter changes during policy transitions. The modified forgetting factor is introduced, and the weighted sum of squared prediction errors for each MPC cycle becomes:

$$J_{MPC} = \alpha_{MPC}^{1}\cdot\left[\alpha_{WBC}^{N^*-2}\cdot e^2\ (1) \cdots \alpha_{WBC}^{1}\cdot e^2\ (N^*-1)\right]\cdot 1_{(N^*-1)\times 1} + e^2\ (N^*) \tag{18}$$

https://doi.org/10.1017/S0263574725103044 Published online by Cambridge University Press

Combining Eq. (17) and (20), we obtain:

$$J(N) = \begin{bmatrix} \alpha_{MPC}^{n^*-1} \cdot J_{MPC}(1) & \cdots & \alpha_{MPC}^{1} \cdot J_{MPC}(n^*) \\ \alpha_{WBC}^{N-n^*N^*-1} \cdot e^2(n^*N^*+1) & \cdots & e^2(N) \end{bmatrix} \cdot 1_{N\times 1} \tag{19}$$

where n^* represents the number of MPC executions. Through this design, whenever the robot's MPC policy updates, the system dynamically decreases the value of the forgetting factor α, thereby achieving exponential decay weighting of historical data while correspondingly increasing the weight of new data. This dynamic adjustment mechanism enables the force estimation algorithm to rapidly track dynamic parameter changes induced by new MPC strategies, significantly improving response capability to external disturbances while ensuring system stability.

4. Adaptive-force-based control

Building upon the hierarchical control architecture described in Section 2, this section details an innovative adaptive force control integration method. The framework achieves real-time compensation and dynamic adaptation to unknown environmental interaction forces by deeply embedding external force estimation into the MPC-WBC control loop, significantly enhancing the stability and adaptability of quadruped mobile manipulation platforms in complex interactive tasks.

4.1. Whole-body control extension

While traditional WBC can handle basic dynamic constraints, their performance often degrades when facing unknown external disturbances. This study enhances WBC in three key aspects:

First, by treating the external force $\lambda_{ee} = (f_{ee}, \tau_{ee}) \in \mathbb{R}^6$ acting on the end-effector as a disturbance term in the centroidal momentum equation, the centroidal dynamics undergo the following modification:

$$\begin{bmatrix} M_b(q) & -J_b^T \end{bmatrix} \cdot x_{WBC} = -h_b(q, \dot{q}) + J_{ee}^T \cdot \lambda_{ee} \tag{20}$$

where J_{ee} is the Jacobian matrix of the robotic arm's end-effector. By treating the external force λ_{ee} acting on the end-effector as a disturbance term and incorporating it into the Task: Equations of Motion, this enhancement enables the system to accurately reflect actual force conditions. Secondly, regarding constraint handling, we have reformulated the Joint Torque Saturation Task:

$$\begin{bmatrix} M_j(q) & -J_j^T \\ -M_j(q) & J_j^T \end{bmatrix} \cdot x_{WBC} \le \begin{pmatrix} \tau_{\max} \cdot 1_{n_a\times 1} - h_j(q, \dot{q}) + J_{ee}^{\tau} \cdot F_{ee} \\ -\tau_{\min} \cdot 1_{n_a\times 1} + h_j(q, \dot{q}) - J_{ee}^{\tau} \cdot F_{ee} \end{pmatrix} \tag{21}$$

This formulation ensures joint torque commands satisfy hardware limitations even under external force disturbances. Finally, a compensation term is introduced in the torque computation step, yielding the ideal joint torque τ^{des} as:

$$\tau^{des} = \begin{bmatrix} M(q) & -J_j^T \end{bmatrix} \cdot {x_{WBC}}^{des} + h_j(q, \dot{q}) - J_{ee}^T \cdot F_{ee} \tag{22}$$

This enhancement enables the WBC to perform real-time compensation for measured external disturbances at 1 kHz control frequency.

4.2. Model predictive control extension

To address the instability of conventional WBC in highly dynamic scenarios, we integrate the extended dynamic model into predictive optimization, combining MPC's predictive capability with WBC's real-time control. The MPC generates reference trajectories accounting for future states, while the WBC performs refined optimization based on real-time dynamic constraints. This framework significantly enhances the dynamic performance of quadruped mobile manipulation platforms when handling unknown end-effector loads, enabling rapid stabilization under disturbances.

During robot-environment interaction, the end-effector experiences both linear contact forces and contact torques τ_{ee}. To accurately model this complete interactive dynamics, we systematically extend

https://doi.org/10.1017/S0263574725103044 Published online by Cambridge University Press

Table I. *Algorithm runtime.*

	Cycle index	Average cycle duration	Average algorithm runtime
Time(ms)	39,957	0.59934	2.5×10^{-5}

the momentum balance equations within the original single rigid-body dynamics framework:

$$\begin{cases} \dot{p}_G = \sum_{i=1}^{n_c} f_i + \lambda_{ee} + mg, i \in N_{contact} \\ \dot{l}_G = \sum_{i=1}^{n_c} r_{Gi} \times f_i + r_{Gee} \times \lambda_{ee} + \tau_{ee} \end{cases} \tag{23}$$

where $\lambda_{ee} = [f_{ee}\ \tau_{ee}]^T \in \mathbb{R}^6$ denotes the end-effector force and r_{Gee} denotes the position of the end-effector relative to the CoM. The input vector is extended to include $u = (\lambda_{c_1}, \cdots, \lambda_{c_{n_c}}, \lambda_{ee}, v_j) \in \mathbb{R}^{3n_c+6+n_a}$.

In formulating the optimization problem, equality constraints must be applied to the generalized contact forces (including linear force f_{ee} and torque τ_{ee}) at the end-effector to ensure physically plausible interactions:

$$\begin{cases} u_{ee,\lambda} = f_{ee} \\ u_{ee,\tau} = \tau_{ee} \end{cases} \tag{24}$$

Since the cost function already includes an optimization objective for the input terms, we employ a relaxed barrier function method to convert these hard constraints into soft constraints integrated into the cost function. Specifically, the composite cost function is constructed as:

$$L(x(t), u(t), t) = \left\| x_r - x_r^{ref} \right\|_{Q_r}^2 + \left\| u - u^{ref} \right\|_R^2 + \left\| r_{IE} - r_{IE}^{ref} \right\|_{Q_{eep}}^2 + \left\| \xi_{IE} \right\|_{Q_{eeo}}^2 \tag{25}$$

where $u^{ref} = [\, 0_{3n_c}\ \lambda_{ee}\ 0_{n_a}\,]^T \in \mathbb{R}^{3n_c+6+n_a}$ is the extended input vector.

5. Experiments

The experimental validation was conducted on a mobile manipulation platform consisting of a Unitree B1 quadruped robot equipped with a 7-DOF Z1 robotic arm. All algorithmic modules were deployed on a laptop PC (Intel i7-9750H, 2.6 GHz) and implemented in the Gazebo 11 simulation environment via the ROS Noetic framework. The system employs the OCS2 open-source rigid-body dynamics library [27, 28] for high-fidelity dynamic modeling. All of the examples discussed in this letter are also included in the supplementary video submission (https://youtu.be/KNBjoGdoA5c).

5.1. Force estimation performance validation

As shown in Figure 3, during this experiment, the end-effector grasped a 1 kg counterweight while the robot maintained stationary standing. Based on local gravitational acceleration (9.8 m/s^2), the nominal external force acting on the robot was 9.8 N.

Comparative analysis of the z-axis force estimation results (Figure 3) reveals that both the traditional method and the α-adaptive method converge near the theoretical value, confirming algorithmic correctness. Notably, the α-adaptive method demonstrates faster convergence compared to traditional methods. These improvements primarily stem from its innovative dynamic forgetting factor adjustment mechanism and deep coupling design with the WBC controller. The performance enhancement significantly boosts the robot's adaptability in unstructured environments, providing reliable technical support for subsequent complex interaction tasks. Experimental data fully validate the dual advantages of the proposed method in both response speed and estimation accuracy, with steady-state estimation mean values deviating <5% from theoretical values.

https://doi.org/10.1017/S0263574725103044 Published online by Cambridge University Press

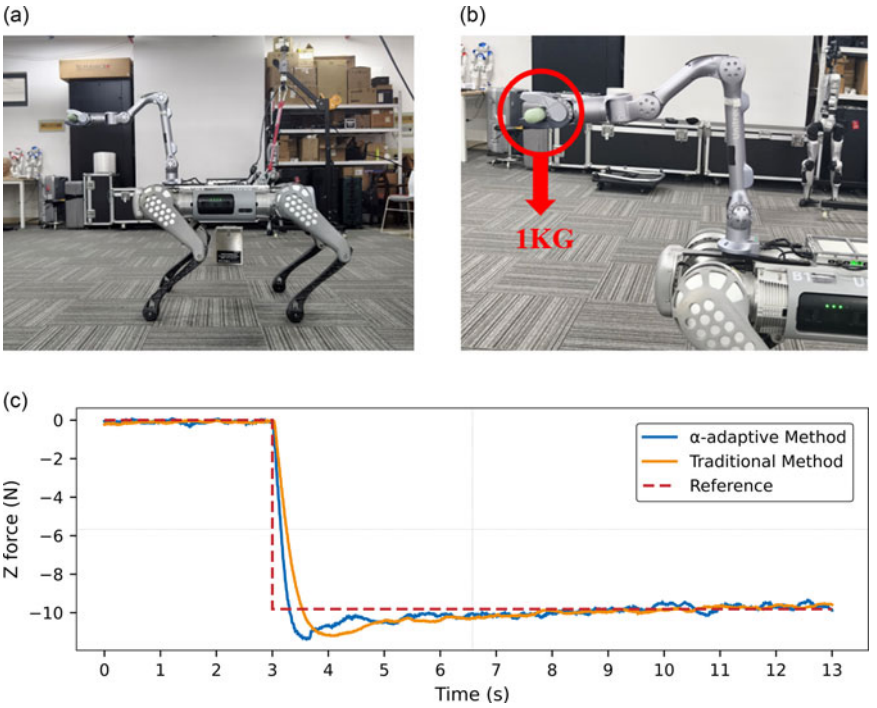


Figure 3. *A performance comparison between the conventional method and the α-adaptive method.*

Furthermore, as detailed in Table I, we conducted a comparative analysis of the computational time consumption for the WBC control loop with the external force estimation module. Experimental results demonstrate that after integrating the force estimation algorithm, the average computation time per control cycle increased by only 2.5×10^{-5} ms. This marginal increment remains entirely within the permissible range of the 1 ms control period, ensuring the system's capability to stably maintain 1000 Hz high-frequency control.

5.2. Algorithm comparison

To systematically evaluate the performance of the proposed adaptive control algorithm, comparative experiments were conducted with the non-adaptive method from ref. [21]. The experimental setup involved a mobile manipulation platform performing in-place stepping motions while monitoring end-effector positional changes under time-varying step loads (20N, 25N, 30N, 35N) applied at the end-effector, with all tests completed in Gazebo simulation environment for safety considerations.

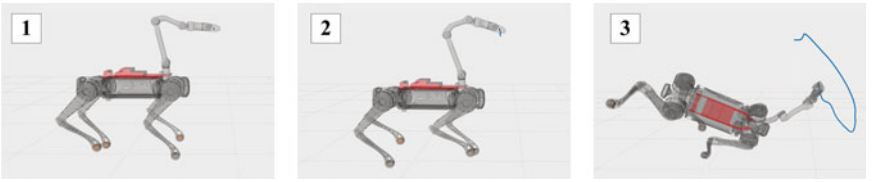
Experimental results (Figures 4, 5) demonstrate the proposed algorithm's superior performance: in terms of robustness, it maintains excellent trajectory tracking performance under full load conditions with end-effector position deviations controlled within ±1cm; regarding stability, it successfully handles sudden 35N loads while maintaining stable system operation; comparative algorithm performance shows the non-adaptive method exhibited significant Z-axis deviation (>5 cm) at just 20N load, ultimately leading to system instability.

5.3. Trajectory tracking under time-varying forces

This experiment validated the effectiveness of the proposed adaptive control algorithm in handling force uncertainties through a challenging non-homogeneous object manipulation task. As shown in Figure 6,

https://doi.org/10.1017/S0263574725103044 Published online by Cambridge University Press

(a)



1. Robot with none-adaptive controller starts in a trot mode. **2.** The end-effector is subjected to a 20 N force at z axis. **3.** The force increased to 25 N, causing the robot to topple.

(b)



1. Robot with adaptive controller starts in a trot mode. **2.** The endeffector is subjected to a 25 N force at z axis. **3.** The force is increased to 35 N, yet the robot maintain stability.

Figure 4. *Compare the postural changes of the robot under adaptive and non-adaptive control.*

the quadruped mobile manipulation platform successfully completed grasping and transporting a 2.5 kg non-homogeneous object (with internal rolling balls simulating mass distribution variations).

The results demonstrate that the proposed algorithm maintains excellent control performance under dynamic disturbances, achieving fast and precise positioning at the target location. Notably, the system exhibited stable transportation capability even under harsh oscillatory disturbances caused by suspended weights.

Experimental results demonstrate that the proposed algorithm effectively handles uncertainties in unstructured environments, as evidenced by comprehensive experimental records, thereby providing a reliable technical solution for complex manipulation tasks. Our work builds upon the advanced framework introduced by Jean-Pierre Sleiman et al., inheriting its advantage of a large manipulator workspace. The key contribution of this study lies in overcoming the stability limitation of that framework when dealing with unknown payloads. Our method achieves a trajectory tracking accuracy within ± 2 cm, demonstrating its potential for practical applications in complex interactive scenarios such as warehouse logistics or search-and-rescue operations.

6. Conclusion

This study proposes a novel adaptive force control system for quadruped mobile manipulation platforms, which effectively addresses object uncertainty in grasping tasks through deep integration of RLS-FF-based adaptive force estimation with the MPC-WBC control framework. Experimental results demonstrate significant improvements in force estimation performance compared to conventional methods. The innovative triple-fusion architecture achieves 1000 Hz high-frequency force compensation while maintaining end-effector deviation below 1 cm under 35N impact loads. Validation through 2.5 kg non-homogeneous object manipulation experiments confirms excellent trajectory tracking performance and stable transportation capability, with 75% increased maximum stable load capacity versus baseline methods. These achievements provide an effective solution for robotic manipulation in dynamic environments. Future work will focus on multimodal sensory fusion research, combining vision and force feedback for prior object parameter estimation to further enhance system adaptability and application scope.

https://doi.org/10.1017/S0263574725103044 Published online by Cambridge University Press

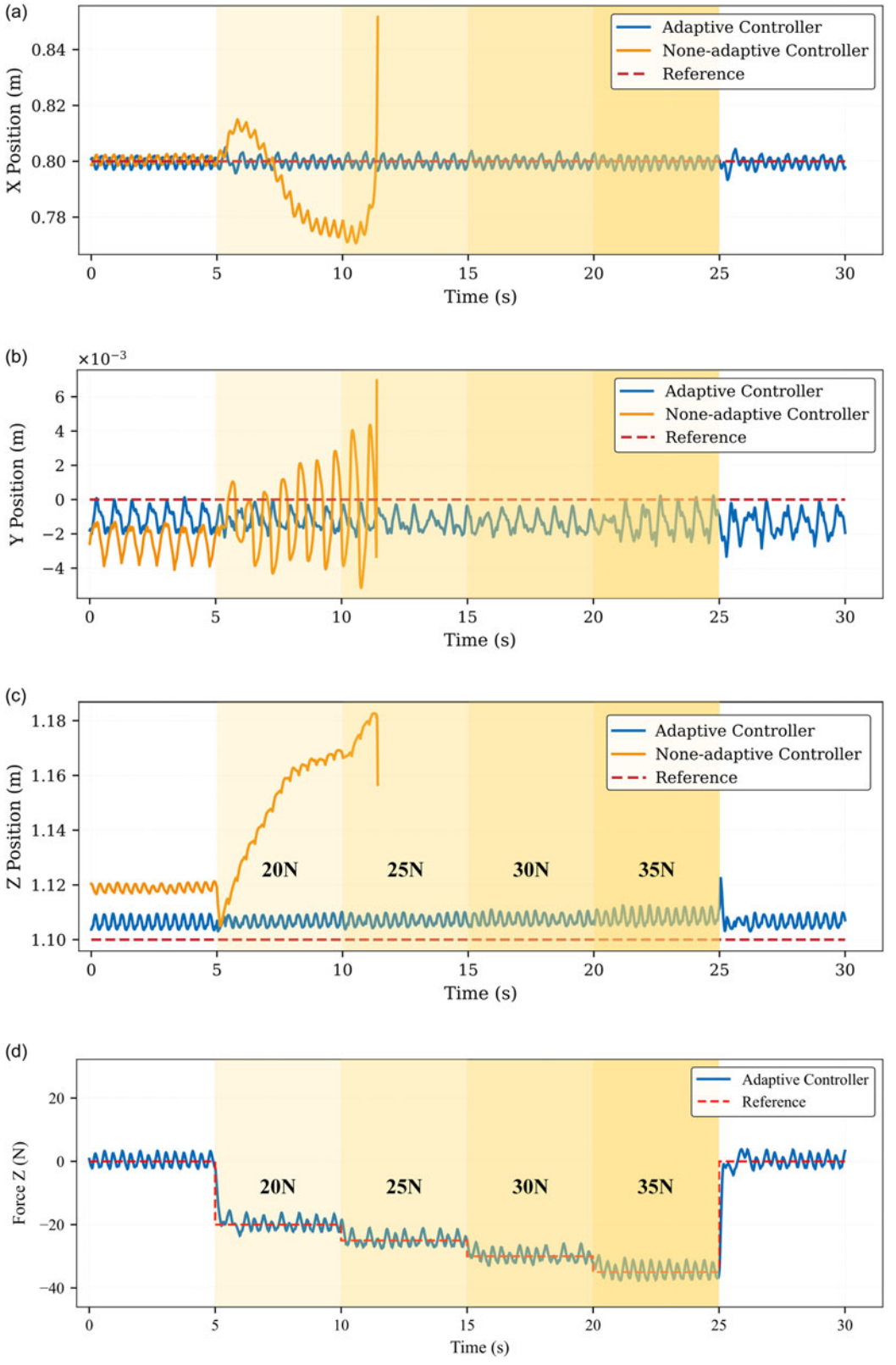


Figure 5. *Comparing performance of adaptive and nonadaptive controllers.*

https://doi.org/10.1017/S0263574725103044 Published online by Cambridge University Press

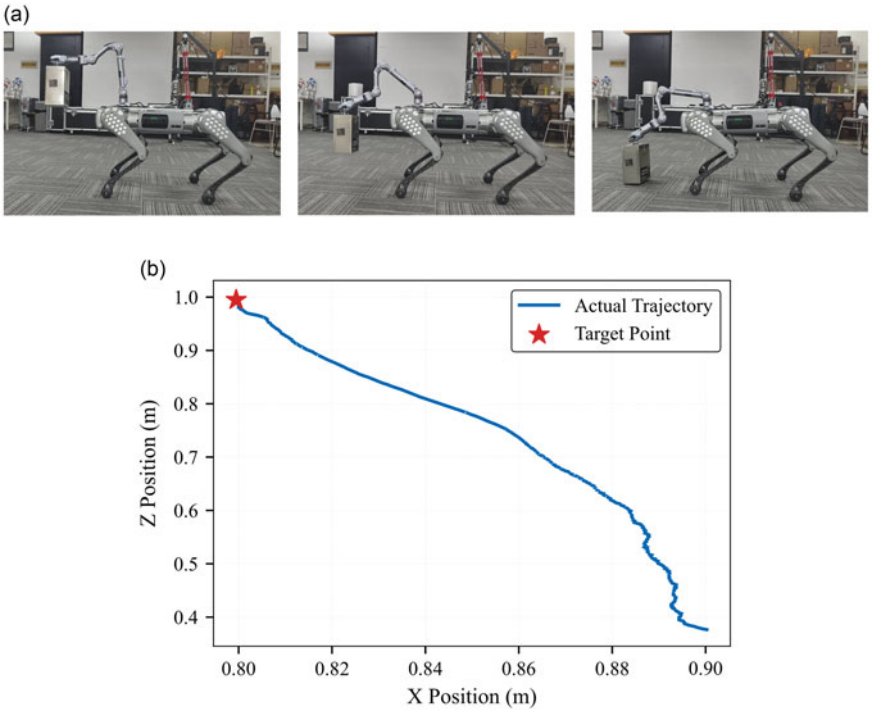


Figure 6. *Successful transportation to target location (0.8 m,1.0 m).*

Author contribution. Zeyu Cai proposed an adaptive force control system for quadruped mobile manipulation platforms. Ruipeng Cai, Zhentao Xie, and Ning Huang provided theoretical guidance, while Qingchuan Li was responsible for text proofreading.

Financial Support. Project supported by the Natural Science Foundation of Zhejiang province, China (No. LD25E050001).

Competing Interests. The author(s) declare(s) that there are no conflicts of interest in this paper.

Ethical approval. None.

References

[1] H. Ferrolho, V. Ivan, W. Merkt, I. Havoutis and S. Vijayakumar, "RoLoMa: Robust loco-manipulation for quadruped robots with arms," *Auton Robot* **47**, 1463–1481 (2023).
[2] S. Zimmermann, R. Poranne and S. Coros. Go Fetch! – Dynamic Grasps using Boston Dynamics Spot with External Robotic Arm. **In:** *2021 IEEE International Conference on Robotics and Automation (ICRA), Xi'an, China* (2021) pp. 4488–4494.
[3] C. D. Bellicoso, K. Krämer, M. Stäuble, D. Sako, F. Jenelten, M. Bjelonic and M. Hutter. ALMA-Articulated Locomotion and Manipulation for a Torque-Controllable Robot. **In:** *IEEE International Conference on Robotics and Automation (ICRA) IEEE* (2019) pp. 8477–8483.
[4] G. Turrisi, L. Schulze, V. S. Medeiros, C. Semini and V. Barasuol, PACC: A passive-arm approach for high-payload collaborative carrying with quadruped robots using model predictive control. **In:** *Proc. IEEE Int. Conf. Intell. Robots Syst* (2024) pp. 11139–11146.
[5] F. Jenelten, J. He, F. Farshidian and M. Hutter, "DTC: Deep tracking control," *Sci. Robot* **9**, eadh5401 (2024).
[6] B. Dynamics, "Spot for safety and incident response," *Youtube* (2024). https://bostondynamics.com/solutions/safety.
[7] Z.-H. Sun, G. S. Yang, B. Zhang and W.-J. Zhang. "On the Concept of the Resilient Machine," **In:** *2011 6th IEEE Conference on Industrial Electronics and Applications, Beijing, China* (2011) pp. 357–360.
[8] J. Di Carlo, P. M. Wensing, B. Katz, G. Bledt and S. Kim. Dynamic Locomotion in the MIT Cheetah 3 Through Convex Model-Predictive Control. **In:** *Proc. IEEE Int. Conf. Intell. Robots Syst* (2018) pp. 7440–7447.
[9] Q. Nguyen, M. J. Powell, B. Katz, J. D. Carlo and S. Kim. Optimized Jumping on the MIT Cheetah 3 Robot. **In:** *Proc. IEEE Int. Conf. Robot. Automat.* (2019) pp. 7448–7454.
[10] M. Focchi, A. del Prete, I. Havoutis, R. Featherstone, D. G. Caldwell and C. Semini, "High-slope terrain locomotion for torque-controlled quadruped robots," *Auton. Robots* **41**(1), 259–272 (2017).

https://doi.org/10.1017/S0263574725103044 Published online by Cambridge University Press

[11] H. W. Park, P. M. Wensing and S. Kim, "Online planning for autonomous running jumps over obstacles in high-speed quadrupeds, Proc," *Robot.: Sci. Syst* **11**, 1–9 (2015).
[12] H. W. Park, P. M. Wensing and S. Kim, "High-speed bounding with the MIT Cheetah 2: Control design and experiments," *Int. J. Robot. Res.* **36**(2), 167–192 (2017).
[13] M. Hadian, W. J. Zhang and D. Etesami, "A robust interpolated model predictive control based on recurrent neural networks for a nonholonomic differential-drive mobile robot with quasi-LPV representation: Computational complexity and conservatism," *Int. J. Syst. Sci.* **55**(15), 3257–3271 (2024).
[14] S. Katayama and T. Ohtsuka, "Whole-body model predictive control with rigid contacts via online switching time optimization," **In:** *Proc. IEEE Int. Conf. Intell. Robots Syst* (2022) pp. 8858–8865.
[15] C. Mastalli, S. P. Chhatoi, T. Corbéres, S. Tonneau and Vijayakumar S., "Inverse-dynamics mpc via nullspace resolution," *IEEE Trans. on Robot.* **39**(4), 3222–3241 (2023).
[16] O. Khatib, "A unified approach for motion and force control of robot manipulators: The operational space formulation," *IEEE J. Robot. Automat.* **3**(1), 43–53 (1987).
[17] S. Kuindersma, F. Permenter and R. Tedrake, "An efficiently solvable quadratic program for stabilizing dynamic locomotion," **In:** *IEEE International Conference on Robotics and Automation (ICRA) IEEE* (2014) pp. 2589–2594.
[18] C. D. Bellicoso, C. Gehring, J. Hwangbo, P. Fankhauser and M. Hutter. Perception-less terrain adaptation through whole body control and hierarchical optimization. **In:** *Proc. 16th IEEE-RAS Int. Conf. Humanoid Robots, Humanoids* (2016) pp. 558–564.
[19] R. Grandia, F. Jenelten, S. Yang, F. Farshidian and M. Hutter, "Perceptive locomotion through nonlinear model-predictive control," *IEEE Trans. Robot.* **39**(5), 3402–3421 (2023).
[20] T. Flayols, A. D. Prete, P. Wensing, A. Mifsud, M. Benallegue and O. Stasse, "Experimental Evaluation of Simple Estimators for Humanoid Robots," **In:** *IEEE-RAS Int. Conf. Humanoid Robot* (2017) pp. 889–895.
[21] J.-P. Sleiman, F. Farshidian, M. V. Minniti and M. Hutter, "A unified mpc framework for whole-body dynamic locomotion and manipulation," *IEEE Robot. Autom. Lett.* **6**(3), 4688–4695 (2021).
[22] Unitree, Z1 SDK Development Guide. [Online]. https://support.unitree.com/home/en/Z1_developer/param.
[23] C. D. Bellicoso, C. Gehring, J. Hwangbo, P. Fankhauser and M. Hutter. "Perception-Less Terrain Adaptation Through Whole Body Control and Hierarchical Optimization," **In:** *IEEE-RAS. 16th International Conference on Humanoid Robots (Humanoids). IEEE* (2016) pp. 558–564.
[24] G. Xin, W. J. Wolfslag, H.-C. Lin, C. Tiseo and M. N. Mistry, "An optimization-based locomotion controller for quadruped robots leveraging cartesian impedance control," *Front. Robot. AI* **7**, 48 (2020).
[25] V. Barasuol, J. Buchli, C. Semini, M. Frigerio, E. R. De Pieri and D. G. Caldwell, "A reactive controller framework for quadrupedal locomotion on challenging terrain," **5**, 2554–2561 (2013).
[26] E. M. Hoffman, A. Laurenzi, L. Muratore, N. G. Tsagarakis and D. G. Caldwell. Multi-Priority Cartesian Impedance Control Based on Quadratic Programming Optimization. **In:** *2018 IEEE International Conference on Robotics and Automation (ICRA)* (2018) pp. 309–315.
[27] OCS2: An open source library for optimal control of switched systems. [Online]. https://github.com/leggedrobotics/ocs2.
[28] J. Carpentier, G. Saurel, G. Buondonno, J. Mirabel, F. Lamiraux, O. Stasse and N. Mansard, "The Pinocchio C++ library: A fast and flexible implementation of rigid body dynamics algorithms and their analytical derivatives," *IEEE/SICE Int. Symp. Syst. Integrat.* (2019) pp. 614–619.
[29] F. Farshidian, M. Neunert, A. W. Winkler, G. Rey and J. Buchli. "An Efficient Optimal Planning and Control Framework for Quadrupedal Locomotion," **In:** *2017 IEEE International Conference on Robotics and Automation (ICRA), Singapore* (2017) pp. 93–100.
[30] F. Farshidian, E. Jelavic, A. Satapathy, M. Giftthaler and J. Buchli. "Real-Time Motion Planning of Legged Robots: A Model Predictive Control Approach," **In:** *17th IEEE-RAS International Conference on Humanoid Robotics, Humanoids, UK* (2017) pp. 577–584.
[31] E. Todorov and W. Li, "A generalized iterative LQG method for locallyoptimal feedback control of constrained nonlinear stochastic systems," *Proc. Amer. Control Conf.* **1**, 300–306 (2005).
[32] R. Grandia, F. Farshidian, R. Ranftl and M. Hutter. "Feedback MPC for Torque-Controlled Legged Robots," **In:** *IEEE/RSJ International Conference on Intelligent Robots and Systems* (2019) pp. 4730–4737.
[33] J.-P. Sleiman, F. Farshidian and M. Hutter, Constraint handling in continuous-time ddp-based model predictive control. **In:** *IEEE International Conference on Robotics and Automation (ICRA)* IEEE (2021) pp. 8209–8215.
[34] M. Zanon and S. Gros, "Safe reinforcement learning using robust MPC," *IEEE Trans. Automat. Control* **66**(8), 3638–3652 (2020).
[35] J. Carpentier and P.-B. Wieber, "Recent progress in legged robots locomotion control," *Curr. Robot. Rep.* **2**(3), 231–238 (2021).
[36] A. Meduri, P. Shah, J. Viereck, M. Khadiv, I. Havoutis and L. Righetti, "Biconmp: A nonlinear model predictive control framework for whole body motion planning," *IEEE Trans. Robot.* **39**(2), 905–922 (2023).

Cite this article: Z. Cai, R. Cai, Z. Xie, N. Huang and Q. Li (2026). "Load-adaptive control for quadruped mobile manipulation platforms", Robotica **44**, 195–209. https://doi.org/10.1017/S0263574725103044

https://doi.org/10.1017/S0263574725103044 Published online by Cambridge University Press